Correlating optical damage threshold with intrinsic defect populations in fused silica as a function of heat treatment temperature

N. Shen, M. Matthews, S. Elhadj, P. Miller, A. J. Nelson, J. Hamilton

November 26, 2012

Disclaimer

This document was prepared as an account of work sponsored by an agency of the United States government. Neither the United States government nor Lawrence Livermore National Security, LLC, nor any of their employees makes any warranty, expressed or implied, or assumes any legal liability or responsibility for the accuracy, completeness, or usefulness of any information, apparatus, product, or process disclosed, or represents that its use would not infringe privately owned rights. Reference herein to any specific commercial product, process, or service by trade name, trademark, manufacturer, or otherwise does not necessarily constitute or imply its endorsement, recommendation, or favoring by the United States government or Lawrence Livermore National Security, LLC. The views and opinions of authors expressed herein do not necessarily state or reflect those of the United States government or Lawrence Livermore National Security, LLC, and shall not be used for advertising or product endorsement purposes.

Correlating optical damage threshold with intrinsic defect populations in fused silica as a function of heat treatment temperature

N Shen, M Matthews, S Elhadj, P E Miller, A J Nelson and J Hamilton

Lawrence Livermore National Laboratory, Livermore, CA 94550

E-mail: nshen@llnl.gov

Abstract. Chemical vapor deposition (CVD) has been used for the production of fused silica optics in high power laser applications. However, relatively little is known about the ultraviolet (UV) laser damage threshold of CVD films and how they relate to intrinsic defects produced during deposition. We present here a study relating structural and electronic defects in CVD films to 355 nm pulsed laser damage threshold as a function of post-deposition annealing temperature (T_{HT}). Plasma-enhanced CVD based on SiH_4/N_2O under oxygen-rich conditions was used to deposit 1.5, 3.1 and 6.4 μm thick films on etched SiO_2 substrates. Rapid annealing was performed using a scanned CO_2 laser beam up to $T_{HT}\sim2100$ K. The films were then characterized using X-ray photoemission spectroscopy (XPS), Fourier transform infrared spectroscopy (FTIR), and photoluminescence spectroscopy (PL). A gradual transition in the damage threshold of annealed films was observed at T_{HT} up to 1600 K, correlating with a decrease in non-bridging silanol and oxygen deficient centers. An additional sharp transition in damage threshold also occurs at ~1850 K indicating substrate annealing. Based on our results, a mechanism for damage-related defect annealing is proposed, and the potential of using high-T_{HT} CVD SiO_2 to mitigate optical damage is also discussed.

1. Introduction

Interest in using high energy laser systems has grown over the years for applications such as inertial confinement fusion [1-2]. The peak power that can be sustained by such laser systems is typically limited by the amount of laser damage that can be tolerated by components making up the optical delivery system. All optical materials, most notably fused silica, have intrinsic absorption properties that will ultimately lead to damage at sufficiently high laser intensities. In practice, however, damage at fluences well below the band gap (~9 eV) have been found to limit the performance of even the highest quality optical components [3]. Generally, macroscopic mechanical defects such as micro-fractures and scratches resulting from grinding, polishing, or handling processes have a high propensity to damage [4-5]. Broadband photoluminescence (PL) from electronic transitions has been observed from these structures but with much shorter life-time than the known point intrinsic defects [4]. At the same time, intrinsic point defects associated with non-bridging oxygen hole centers (NBOHC) and oxygen deficient centers (ODC) have also been associated to laser damage in silica [6] [7] [8]. In addition to these intrinsic defects, extrinsic defects in the form of impurities left by the polishing process, or introduced through environmental contamination, can also lead to absorption of laser light and damage [9]. A deeper understanding of different types of light absorbing defects in silica and methods to mitigate them could shed light on the physics of laser damage processes and facilitate development of more effective damage mitigation strategies.

On the other hand, the optical fiber industry has long enjoyed the benefit of extremely high-purity and low-loss silica, produced through chemical vapor deposition (CVD), which possesses very high damage threshold [10]. Besides high purity, the rapid, high temperature annealing associated with the fiber draw process is also believed to be a key to mitigating defects that may otherwise absorb and lead to damage. Localized CO_2 laser annealing of silica optics at high temperatures has also been demonstrated to greatly improve laser damage thresholds [11-12]. One approach to study the aforementioned intrinsic defects which limit both bulk and surface silica optics performance would be to obtain high purity and optical quality CVD-based SiO_2 and probe the effect of rapid, high temperature annealing on damage threshold. Indeed, very few [13] UV laser damage threshold measurements of CVD silica films have been performed, and we are unaware of any studies in which a SiO_2 capping layer on fused silica was applied as a means to improve damage threshold or mitigate defects.

In this work, we characterize the evolution of UV damage threshold, microstructure and intrinsic defect populations of defect-rich SiO_2 thin films on etched silica substrate as a function of heat treatment temperature (T_{HT}) from focused CO_2 laser heating. High-purity, unannealed SiO_2 films were first deposited using plasma-enhanced (PE) CVD based on SiH_4/N_2O precursor chemistry. Subsequent localized annealing to various heat treatment temperatures is performed using a scanned CO_2 laser beam at 10.6 μm wavelength where the laser energy is efficiently coupled to silica for heating. Laser annealing using CO_2 laser allows rapid heating of silica to very high temperatures without causing devitrification of the glass often seen with isothermal oven annealing above ~1400K [14]. At a scan rate of 50 μm/s, our results indicate a sharp increase in the 355nm, 3ns pulse laser damage threshold for $1600 < T_{HT} < 2000$ K. Spatially and spectrally resolved PL mapping of as-deposited CVD films indicates a high concentration of electronic defects relative to the etched substrate, which are effectively annealed at high T_{HT}. The change in PL versus T_{HT} roughly correlated with that of the intensity of non-bridging silanol modes as

characterized by Synchrotron-based Fourier transform infrared spectroscopy (SR-FTIR). In contrast, the average Si-O-Si bond angle derived from the IR spectra evolved linearly and gradually up to 1600 K, and then stabilizes for T_{HT} >1600 K. These results suggest that mid-range ordering of the silica network, affecting bond angles, is first required for damage precursor healing, followed by short-range ordering which then quenches all available defects involved in damage initiation. In terms of application, the approach of applying rapidly annealed CVD overlayers to mitigate or passivate damage on high power laser optic surfaces is also discussed.

2. Experimental

2.1. Sample preparation

All samples were 10 mm thick, 2" round UV-grade type-III fused silica (Corning 7980). HF-etching was used to remove ~27 μm of surface material to eliminate any polishing contaminants, followed by a standard NaOH/detergent cleaning step, and deionized water rinse [15]. The samples were then piranha-etched (1:1, H_2SO_4:H_2O_4) and coated with SiO_2 using PE CVD method in a SiH_4/N_2O precursor gas at 300 mTorr with a substrate temperature of 573 K. The thickness of the SiO_2 film for each sample and the as-received film laser damage threshold are shown in Table 1. A control sample was HF etched, cleaned, and then piranha etched as described above. Samples were processed at the MicroFabrication facility at LLNL.

Table 1: Sample coating thickness and laser damage threshold.

Sample ID	Film thickness (μm)	R/1 damage threshold (J/cm^2)
M2037 (control)	--	45.3 ± 3.7
M2063	1.5	15.0 ± 1.5
M1105	3.1	22.7 ± 2.0
M2183	6.4	19.9 ± 1.7

While clean room sample handling procedures were used throughout the cleaning and coating steps, some scratches on the uncoated side were produced from wafer carriers. Furthermore, some residue and/or haze was apparent, appearing on both coated and uncoated surfaces; coating-side residue appeared mainly underneath the coating. When characterizing and damage testing the samples later on, we carefully avoided regions with scratches or residue.

2.2. Infrared laser annealing treatments

Localized 10.6 μm laser heating of the silica CVD films deposited on silica was performed as a means of rapid thermal annealing through the absorption of IR light. A Gaussian $1/e^2$ beam diameter of 1 mm with power ranging between ~3 to 6 W allowed for a sufficiently large treatment areas for small-beam (~80 μm in diameter) damage testing and material characterization with optical probes. Scanning was performed at 5 to 50 μm/s by moving the sample stage, producing ~20 mm long tracks. The heat affected zone or the effective annealing zone scales with peak temperatures, beam size, and the effective beam dwell time as determined from the sample translation speed. For instance, for the maximum scan rate used, 50 μm/s, a given point on the sample surface is exposed to >90% of peak treatment temperature rise from a 1 mm beam in about 4.5 s. Because the effective dwell time is long relative to the thermal

diffusion time (τ_{th}~40 ms), the heating depths due to diffusion are large compared with the film thickness. Therefore, the heating across the films is assumed uniform in depth. Details of the laser used for heating and the camera and optical system used for the *in situ* measurements of the *T* spatial profile are available elsewhere [16]. Briefly, a calibrated HgCdTe infrared camera operating at 1 Hz with a narrow bandpass cold filter (λ_c=8.9 μm) was used to capture the infrared blackbody radiation emitted from the IR-laser heated surface, which was then used to resolve the *T* profiles over time from each captured frame. The spatial resolution achieved by the IR thermal imaging system was ~40 μm. Typical temperature profiles are shown in figure 1, from which the effect of temperature and scan rate (dwell time) on annealing can be determined as describe in the following section. The variability in the T_{HT} profiles in mostly due to the fluctuation in the laser power of ~5%. In the results that follow, we report time-averaged (peak or local) heat treatment temperatures for t>4.5 s and up to the laser turn off time unless otherwise noted. Individual laser treatment tracks were made covering a peak temperature range of 1300~2400 K, which corresponds roughly to the range between the glass transition point and the maximum sub-evaporation temperature over the time scales considered here.
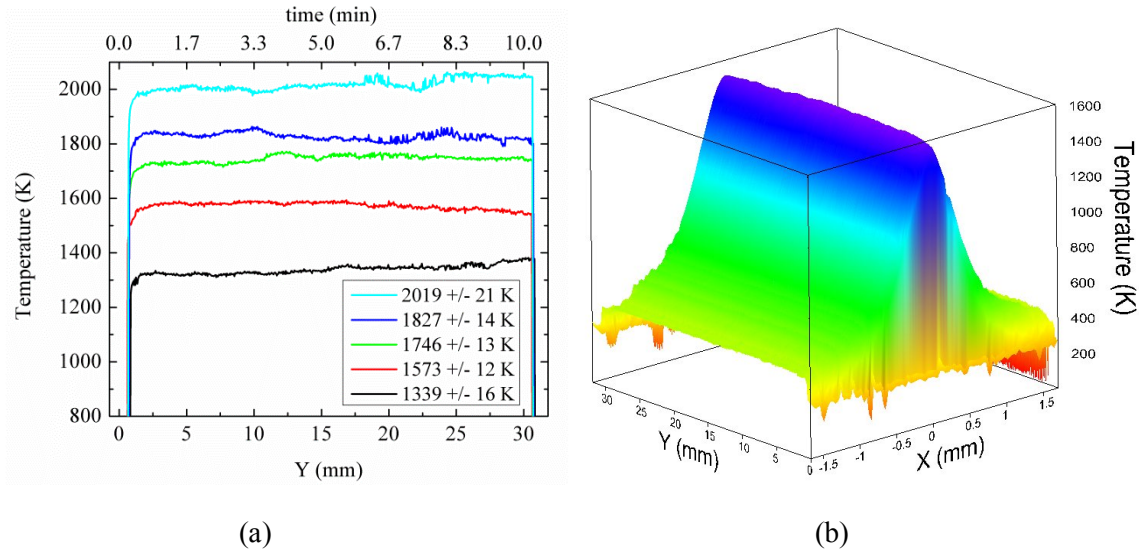

(a)   (b)

Figure 1: Measured temperature data for 50 μm/s laser scanned profiles indicating the relative stability of the peak temperature as a function of time and scan position shown in (A) and the slowly varying spatial profile shown in (B).

2.3. Damage testing and characterization

2.3.1. Infrared Spectroscopy

Fourier transform infrared (FTIR) spectroscopy was used to evaluate the degree of polymerization, silica chemistry and densification of the coatings. Large aperture, fixed angle (~16°) incidence IR reflectance measurements of coatings prior to laser treatment and from 360 to 4000 cm^{-1} were made using a Perkin Elmer Spectrum One system with a resolution of 4 cm^{-1} and accuracy of 0.1 cm^{-1}. Spatially resolved (~10 μm spot size) normal incidence IR reflectance scans of laser-treated regions over the same spectral range were made using a coherent synchrotron radiation source (Advanced Light Source, Lawrence Berkeley National Laboratory) coupled via 32x/0.65NA reflective optics to a Spectra Tech Nic-Plan IR microscope. The synchrotron based FTIR (SR-FTIR) measurements were accurate to 0.09 cm^{-1} with a

resolution of 4 cm^{-1}. A lateral step size of 50 μm was used to measure variations in IR reflectance as a function of local thermal treatment. Additional details of the SR-FTIR system are described elsewhere [8].

2.3.2. R/1 damage testing

The pulsed laser damage resistance of the sample was assessed using small beam R/1 laser damage testing [17]. A Coherent Infinity Q-switched Nd:YAG laser operating at 355 nm was used in the test. The temporal profile of the laser pulse is Gaussian with a FWHM pulse duration of ~3 ns. The laser is focused onto the exit surface of the silica specimen. The laser pulse energy and its spatial profile are monitored by picking off a fraction of the beam and recording it using a charge coupled device (CCD) camera. The Gaussian beam has a measured $1/e^2$ beam radius of r~40 μm which was used to determine peak axial fluence as $\phi=2E/\pi r^2$ where E is the incident pulse energy accounting for reflection loss from the sample. An imaging microscope is set up to observe the sample under laser irradiation. During damage testing, the laser pulse energy is slowly ramped up with ~5 J/cm^2 steps until damage is registered on the imaging CCD camera. Each R/1 damage threshold measurement is the average of ~10 spatially separate damage test sites. Test scans along the CO_2 laser treated tracks excluded the first ~3 mm of the tracks to allow temperature to reach steady-state. Large area damage testing was also performed and used to compliment the small beam testing in the low THT regime. Further results from large area testing will appear in a future publication.

2.3.3. Photoluminescence spectroscopy

Photoluminescence (PL) spectroscopy was used to probe electronic defects in the deposited SiO_2 that are optically-active in the wavelength region where damage thresholds were assessed. For PL excitation, we focused a quasi-CW 351nm laser (Crystalaser, Q-switched Nd:YLF) through a 74x/0.65NA reflective objective onto the sample. Scattering and luminescence excited by the laser are collected by the same objective, then focused onto a 50 μm core multimode fiber and delivered to a Horiba iHR-320 f/4 spectrometer equipped with a Princeton Instruments LN-cooled CCD. The lateral, axial and spectral resolutions of the system were ~10 μm, ~240 μm and ~2 nm, respectively. Scattered laser light was minimized by the use of a dichroic mirror (Delta, Denmark) and a notch filter at 351nm (Kaiser Optical Systems, Inc.).

2.3.4. X-ray photoemission spectroscopy

XPS was used to investigate the surface chemistry of as-deposited CVD film and after CO_2 laser treatment. XPS analysis was performed on a PHI Quantum 2000 system using a focused monochromatic A; $K\alpha$ x-ray (1486.7 eV) source for excitation and a spherical section analyzer. The instrument has a 16-element multichannel detection system. A 100 μm diameter x-ray beam was used for analysis. The x-ray beam is incident normal to the sample and the x-ray detector is at 45° away from the normal. The pass energy was 23.5 eV giving an energy resolution of 0.3 eV that when combined with the 0.85 eV full width at half maximum (FWHM) Al $K\alpha$ line width gives a resolvable XPS peak width of 1.2 eV FWHM. The collected data were referenced to an energy scale with binding energies for Cu $2p_{3/2}$ at 932.72 +/- 0.05 eV and Au $4f_{7/2}$ at 84.01 +/- 0.05 eV. Binding energies were also referenced to the C 1s photoelectron line arising from adventitious carbon at 284.8 eV. Low energy electrons were used for

specimen neutralization. The sample was sputtered for 10 minutes at ~3 kV to remove surface contaminants before XPS data was collected from un-annealed film, and 3 locations along the track of sample M2063 treated at ~1900 K.

3. Results

3.1. Infrared spectroscopy

IR reflectance spectra were taken of the CVD coating following deposition using FTIR, and compared with 'pristine' etched-only surfaces. Figure 2(a) shows a typical far-IR spectra taken of the 1.5 μm thick film sample M2063 between 400 and 1450 cm^{-1}, where 4 of the 5 peaks can all be associated with fundamental Si-O vibrational modes of tetrahedral SiO_2: bridging O atom rocking at 440 cm^{-1}, symmetric stretching Si-O-Si at 790 cm^{-1}, and an asymmetric stretch Si-O-Si mode which shows a strong splitting into a transverse optic (TO) mode at ~1120 cm^{-1} and a longitudinal optic (LO) mode at ~1220 cm^{-1}. We refer to these modes as TO_1, TO_2, TO_3, and LO_3 modes respectively. In addition, a small peak near 900 cm^{-1} is also visible for the as-deposited film only in the far-IR spectrum (see inset of figure 2(a)) which could be assigned to (at least) one of three possible modes previously observed in SiH_4-based films: Si-N stretching mode from unintentional N doping [18], Si-H wagging mode [19] or a Si-O/Si-OH non-bridging stretching mode [20]. However, Si-N can be ruled out based on XPS results presented below which indicates no detectable N in the films, while the Si-H wagging mode should also produce a corresponding Si-H stretching mode at 2265 cm^{-1} which we did not observe in any of the films studied. We therefore assign this peak to the Si-O/Si-OH non-bridging stretching mode created either during synthesis and/or through ambient water absorption post-deposition [21]. Its density is estimated by normalizing the area underneath the peak (figure. 2(a) inset) to the TO_3 mode intensity. Besides the appearance of the non-bridging mode in as-deposited films as compared with a pristine surface, the peak frequency of the TO_3 mode of the former in figure 2(a) shows a large red-shift of 24 cm^{-1} relative to that of the latter. Similarly, smaller (blue-) red-shifts of the (TO_2) TO_1 were observed and equal to (12 cm^{-1}) 16 cm^{-1}. The overall reflectivity of the as-deposited film appears lower as compared to that of the control samples, particularly in the LO-TO asymmetric stretch region (~1100 cm^{-1}). Figure 2(b) shows the mid-IR reflectance spectra in the region of the O-H stretch vibration. For the etched-only control samples a band near 3600 cm^{-1} corresponds to isolated, bound silanol groups (Si-OH) typical of type-III vapor-deposited glasses such as Corning 7980. However, the mid-IR spectra of the unannealed CVD sample (M2063 with 1.5 μm thick film) shows a much broader OH band, indicative of relatively high silanol concentration and interaction between OH groups which acts to soften the vibrational mode [21]. The relatively large contribution of this O-H stretch band would also tend to support the assignment of the Si-OH mode to the ~900 cm^{-1} peak. No peaks in the reflection spectra were observed in the range 1400 – 2600 cm-1. A multi-component Gaussian fit was performed on the FTIR spectra between ~840 and ~1150 cm^{-1} in order to extract the TO_3 frequency. The integrated intensity of the non-bridging mode is estimated by drawing a baseline shown as the dashed line in figure 2(a), and calculated the area underneath.

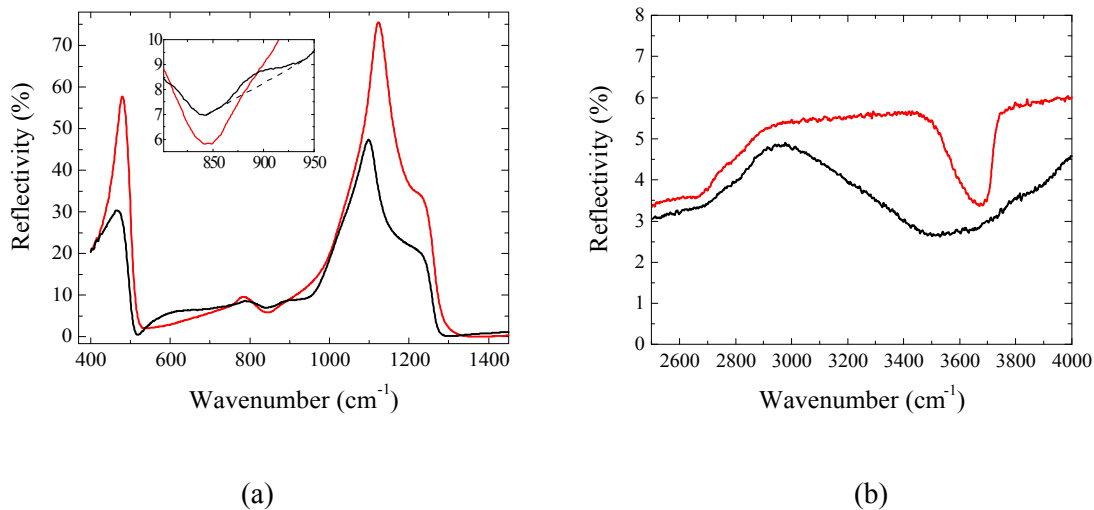(a)   (b)

Figure 2(a) and (b): FTIR spectra of as-deposited CVD film M2063 with 1.5 μm thick film (black curve) and etched-only control sample, M2037 (red curve). The inset of (a) shows the spectral region of the non-bridging mode and the French curve used to approximate the peak area.

Following SiO_2 film deposition, the samples were locally and rapidly annealed along ~1×20 mm tracks using a focused CO_2 laser. Structural changes in the CVD films associated with the laser treatments were recorded using spatially-resolved SR-FTIR microscopy. Lateral scans across each of the laser-treated tracks resulted in spatially-dependent spectra which could be registered with thermal imaging data to yield temperature- and scan rate-dependent spectra. With increasing T_{HT} from laser heating, the polymerization of the CVD films gradually progressed, as observed through the evolution of the FTIR spectrum as shown in figure 3. Referring to figure 3(a), laser annealing appears to lead to a decrease in non-bridging Si-O, Si-OH in general, a blue shift of the TO_1 and TO_3 modes, and a red shift in the TO_2 mode. The total reflectivity also increased as a function of laser annealing. Because the laser treatments induce an increase in fictive temperature [22], the spectra corresponding to the most aggressive thermal treatment did not exactly coincide with that of the pristine substrate. In particular, the TO_3 mode appears at 1120-1122 cm^{-1} for the highest temperature treatments, as compared with 1123 cm^{-1} for the pristine surface indicating a slightly densified final state. The broad LO_3 mode did not appear to shift appreciably in frequency, nor change in intensity relative to the TO_3 mode which indicates that the films remained relatively smooth at the micron scale [23]. Along with changes in the longwave IR region of the fundamental SiO_2 modes, a decrease in OH peak reflectivity in the mid-IR region of film reflectivity also occurred as a function of T_{HT}, as shown in figure 3(b). Although specific sub-features could not be discerned due to the broadness of this band, the highest temperature case shown in figure 3(b) (T_{HT}=2000 K) appears similar to a type-I, low OH silica with OH concentrations of less than 150 ppm by weight.
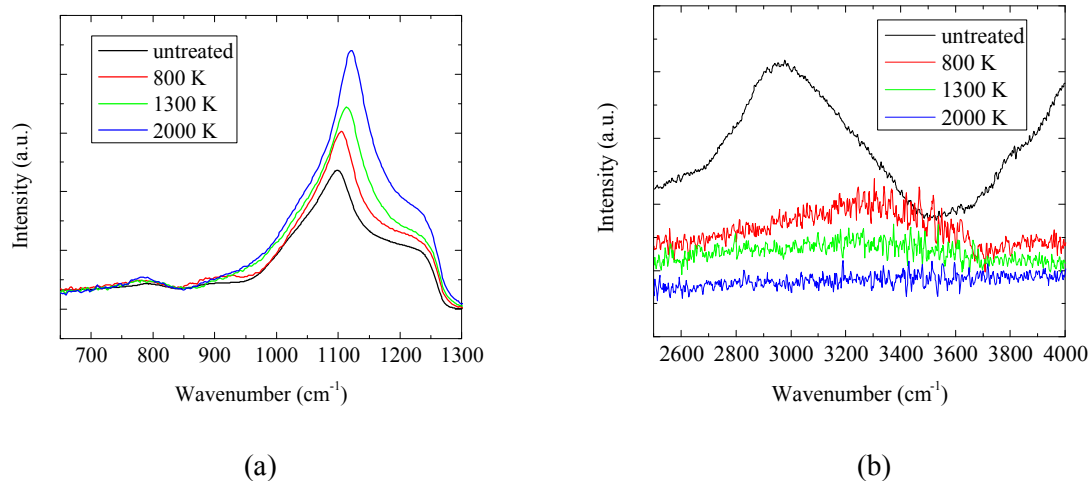
Figure 3: FTIR reflection spectra of CVD sample M2063 with 1.5 μm film following a 50 μm/s CO_2 laser treatment with the evolution of TO frequency (a), and OH vibration (b) at different T_{HT}.

We now quantify the behavior of the CVD film in terms of frequency shift and intensities in figure 4 as a function of T_{HT}. We first note that the Gaussian spatial profile of the CO_2 laser beam creates a continuous varying Gaussian-like temperature profile across each treatment track. Due to the spatial proximity of laser treatment tracks (2 mm spacing between tracks), some small amount of unintentional pre- and/or post-treatment overlap potentially exists at the boundary between tracks measured. The evolution of the TO_3 peak frequency and the non-bridging mode intensity are plotted as a function of the measured *local* T_{HT} for two treatment tracks on 6.4 μm thick film sample M2183, for peak treatment temperatures of 2152 K and 1950 K in figure 4. The monotonic shifting in the TO_3 frequency between 500 and 1500 K indicates the continuous relaxation of the glass network and approaches maximum value close to pristine glass at ~1600 K. The intensity of the non-bridging mode, on the other hand, decreases first at low T_{HT}, but increases at higher T_{HT}, peaking at ~1600 K (dashed line in figure 4) before a steep drop at higher treatment temperature.
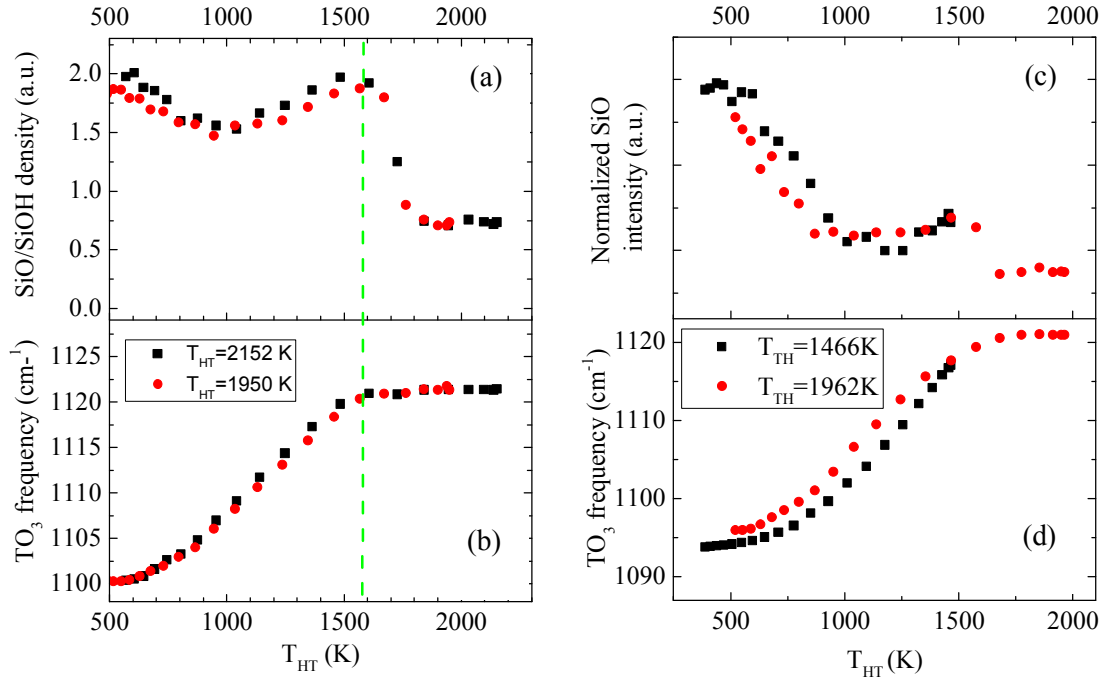
Figure 4: Evolution of the normalized intensity of the non-bridging mode (a) and frequency of the asymmetric TO_3 mode (b) across two individual laser treatment tracks on sample M2183 (6.4 μm thick film); and two tracks on sample M1105 (3.1 mm thick film) in panel (c) and (d). The dashed line indicates the transition point observed in the PL measurements in figure 6 and the damage threshold measurements of figure 7.

We also examined the sample M1105 with 3.1 μm film, and found the TO_3 frequency behaving similarly to the thicker 6.4 μm film with respect to T_{HT} shown in figure 4(c). The non-bridging mode intensiy (figure 4(d)) also drops for $T_{HT}<1000$ K, but does not recover as much as the thicker film. The frequency shifts of the TO_3 mode for all the laser treatment tracks on the three samples used in our study are summarized in figure 5 as a function of the peak T_{HT}. The dashed line is an overlay of the local TO_3 frequency across a single treatment track with the peak T_{HT} of 2152 K and appearing in figure 4. The composite data is noisier as expected due to sample and local CVD deposition variability, but agrees reasonably well with the result from the single track measurement.
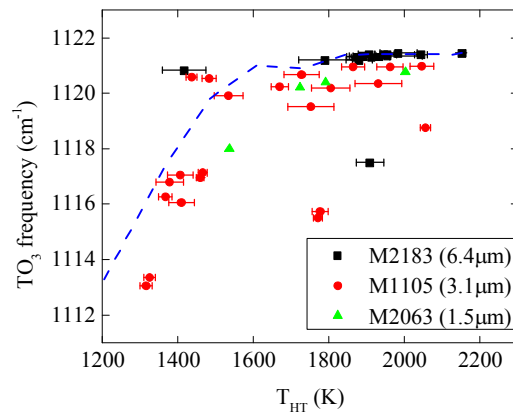
Figure 5: Frequency shift of the TO_3 mode for all treatment tracks on three samples as a function of peak T_{HT} averaged along the tracks. The dashed line is an overlay of the local TO_3 frequency data from figure 4(a) at T_{HT} =2152 K.

3.2. Photoluminescence spectroscopy

The presence of a non-bridging mode in the FTIR reflectance spectra suggested there may be a population of optically-active non-bridging oxygen hole centers in the CVD films that have previously been associated with optical damage [8, 24]. In order to observe more directly the electronic transitions that may be associated with these defect vibrational states, we performed photoluminescence spectroscopy with 351 nm laser excitation, and focused on the PL spectra range between 400 to 670 nm in our analysis. Also, PL from the CVD film was sensitive to photobleaching which limited the dwell time at, and distance between, each data point during our scan. Instead of matching the 50 μm steps used in the FTIR measurements, we scanned the sample with 100 um steps for the PL. A set of three representative PL spectra taken across a single CO_2 laser treated track on sample M2183 with 6.4 μm thick film is shown in figure 6(a). The maximum T_{HT} reached at the center of this treatment track was ~2100 K. The local T_{HT} on the track ~200 μm away from the treatment center was ~1800 K based on the thermal camera measurements. "Untreated" region in figure 6 refers to the location sufficiently far from the treatment track where the CVD film was not exposed to elevated temperatures above room temperature. The spectra were then fitted with multiple Gaussian peak functions to help identify SiO_2 defects that give rise to the photoluminescence signal. The broad emission peak centered ~450 nm is associated with the well-known SiO_2 defect of oxygen deficiency center ODCII ($\equiv$Si…) [25]. Although the excitation of the non-bridging oxygen mode is not efficient at 351nm, it is still surprising that PL from the non-bridging Si-O typically observed ~650 nm was absent despite seeing significant non-bridging mode contributions in corresponding the FTIR spectra. However, this observation is consistent with the relatively large contribution of O-H stretch vibrations and the notion that most of the non-bridging structures are either terminated as silanol groups (…H-O-Si$\equiv$) or otherwise passivated in terms of electronic transitions. In terms of the total defect concentration – and inferred broadband PL intensity – we expect a gradual decrease as the films transition to a higher damage threshold state. Interestingly, the total PL signal first increased, then decreased with T_{HT}, in contrast to the monotonic increase in bridging mode frequency revealed by SR-FTIR but somewhat correlated with the non-bridging oxygen mode intensity. This effect is more clearly seen in figure 6(b) where the PL intensity at the ODC defect peak is plotted as a function of the local T_{HT} across laser treatment tracks.
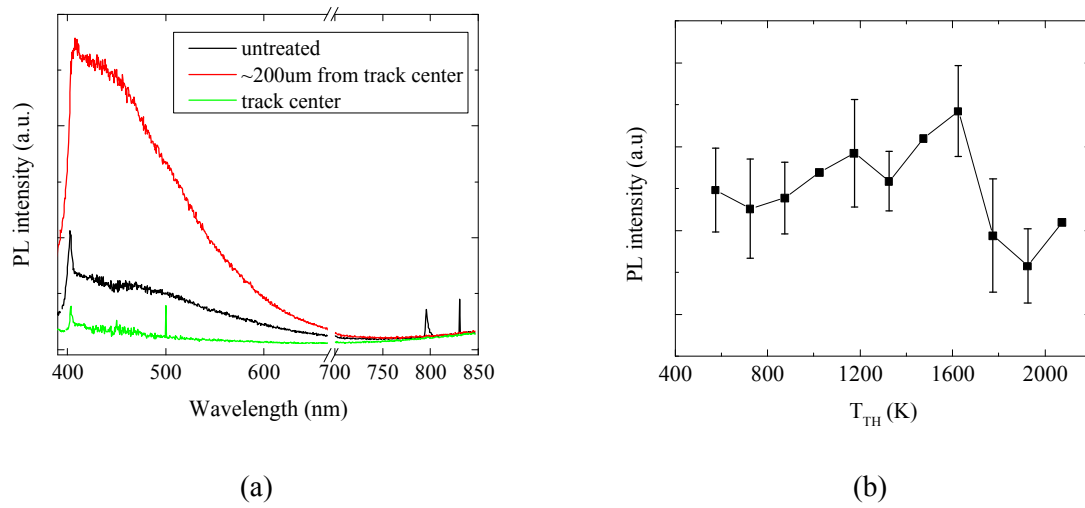
Figure 6: (a) Photoluminescence spectra taken at three locations on sample M2183: in an untreated area, ~200 μm from a laser treatment track and at a track center where T_{HT}=~2100; (b) PL intensity of the CVD film as a function of local treatment temperature across three representative tracks.

3.3. R/1 laser damage test

Damage thresholds of the CVD film were first measured prior to CO_2 laser treatment (Table 1). Samples were then treated with varying CO_2 laser power (i.e. temperature) from ~3 to 6W and scan rate (i.e. dwell time) and retested. Figure 7(a) shows the normalized R/1 damage threshold as a function of the peak T_{HT} at the center of the tracks with a scan rate of 50 μm/s. For T_{HT}<1500 K, the damage threshold did not appear to change significantly. However, a very sharp transition in damage threshold behavior is observed in the range 1500<T_{HT}<1700 K for the 1.5 and 3.1 μm thick films, where the normalized damage threshold improves roughly 2 times, corresponding to changes from the as-deposited value of ~17 J/cm^2 to ~40 J/cm^2, close to the value of the underlying substrate. Above ~1750 Kall three samples show a transition where the normalized damage threshold increases another fold to ~65 J/cm^2, well in excess of that of the underlying substrates. We examined two T_{HT} points – 1200 and 1500 K – for the 1.5 μm film of sample M2063 that are near- or sub-threshold along the S-curve in figure 7(a) and observe the R/1 behavior as a function of slower scan rates. The results are shown in figure 7(b), cast in terms of inverse scan rate where scan rates ranged from 5 to 50 μm/s. The R/1 damage threshold at zero inverse scan rate (infinite scan rate) is taken as the untreated threshold value (~17 J/cm^2). At T_{HT}=1200 K, which is just below the glass transition temperature (T_g) for type III silica of ~1300 K, an increase in damage threshold is observed below a scan rate of 10~25 μm/s (effective dwell time of ~1-2.3 s), although the threshold increase apparently plateaus at ~30 J/cm^2. A similar increase is observed at T_{HT}=1500 K, with a higher threshold scan rate of >50 μm/s, and an additional increase in going from 10 to 5 μm/s.
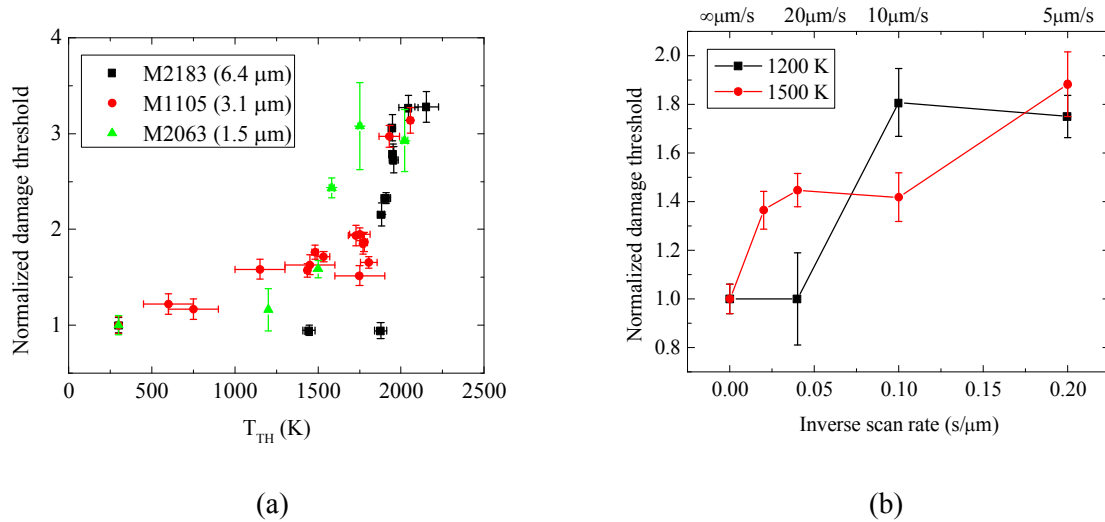
Figure 7: Normalized R/1 damage threshold measurements of the test samples as a function of T_{HT} (a) and as a function of scan rate at 1200 and 1500 K (b).

3.4. X-ray photoemission spectroscopy

XPS was used to assess stoichiometry, verify purity and probe the Si and O electronic states of the films which are in general sensitive to local electronic enviroments. Table 2 summarizes the XPS compositional analyses for the CO_2 treated track and the untreated background. No residual nitrogen from the N_2O precursor gas was detected in the CVD film (detection sensitivity 1019 cm^{-3}). Minimal carbon contamination was only detected on the untreated CVD film likely due to organic contaminant from the environment, exacerbated by the porous nature of the film.

Table 2: Elemental analysis from XPS measurements

Area	Si	O	C	O/Si
Untreated CVD film	32.05	66.05	1.90	2.06
CO_2 laser treated CVD film	32.67	67.33	-	2.06

Figure 8 compares the Si $2p_{3/2,1/2}$ spectra of the as deposited PVCVD and the laser treated track of sample M2178. A single peak near 104 eV was observed corresponding to the Si4+ oxidation state associated with SiO2 [26]. The Si $2p_{3/2,1/2}$ spin-orbit components were deconvolved and are centered at 103.3 and 104.0 eV for the as-deposited films. A small shift in the Si $2p_{3/2,1/2}$ spin-orbit components was observed for the laser treated area to 103.5 eV and 104.2 eV typical for pure SiO_2 (NIST XPS database), FWHM remaining the same. Correlating this chemical shift with the compositional analysis indicates that the laser treated areas have a composition and structure closer to that of bulk SiO_2 than the untreated film, consistent with the improved damage thresholds.
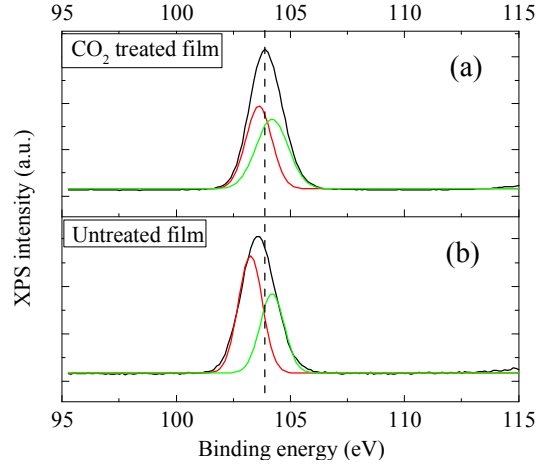
Figure 8: Si 2p binding energy of (a) laser-treated region corresponding to a peak temperature of 1900 K and (b) as-deposited CVD film measured by XPS.

4. Discussion

The presence of both extrinsic (i.e. contaminant) and intrinsic defects in the silica films can lead to absorption and subsequent damage initiation under UV illumination as compared with pristine, etched silica substrates. Furthermore, if the CVD films contain nano-fractures undetectable to our instruments, the decrease in mechanical strength of the film could also lead or add to a reduction in damage threshold. Since the purity of the films in our study was reasonably high, and the damage threshold increases upon CO_2 laser heating, this suggests that the extrinsic defects are not the dominant damage precursors in the CVD films. The intrinsic defect concentration, however, was relatively high for the as-deposited films, as probed by both PL and FTIR measurements. The change in defect-related spectra also correlates well with the change in damage threshold of the film as it was being treated with CO_2 laser. We therefore believe the intrinsic defects are the main contributors to laser light absorption and damage.

Shifts in the peak positions in the infrared reflectivity spectra can be related to physical variation in internal structure of the glass network such as the number of 3- and 4-member Si-O rings, average Si-O-Si bond-angle and density. For example, as-deposited vapor-based silica films are expected to have densities lower than that of annealed films due to a high porosity driven by the presences of large voids and accompanying defects. The average Si-O-Si bond angle can be estimated using the central force network model [27],

$$\omega^2 = \frac{k}{m_o}(1 - cos\theta) + \frac{4}{3}\frac{k}{m_{si}}$$

where ω is the angular frequency of the TO_3 mode, k is the Si-O stretching force constant, θ is the average Si-O-Si bridging angle, and m_o and m_{si} are the mass of the oxygen and silicon atoms. With increasing laser-heat-treatment and increasing polymerization of the films, the bond-angle relaxes, and the density decreases through the annihilation of non-bridging oxygen structural defects, producing a rise in damage threshold (figure 9). As a prelude to this damage threshold increase, however, an increase in IR reflectivity due to non-bridging oxygen or silanol groups is observed. An increase in IR activity of this

band would be consistent with an increase in the more dipolar O- over OH structures as water and hydrogen are driven out during annealing, leading the way for bond-bridging. An increase in dipole strength due to non-bridging oxygen could also bring about a more intense ODC PL emission through a decrease in PL lifetime.
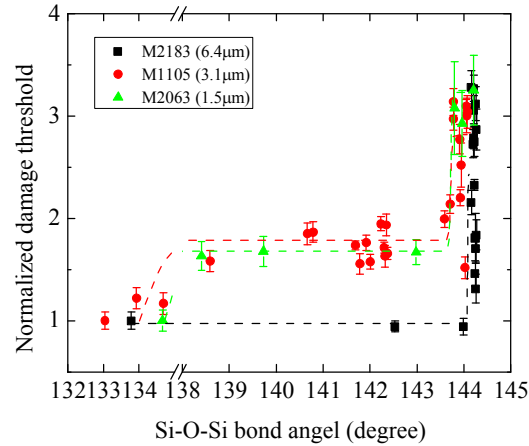

Figure 9: R/1 damage threshold measurements of three test samples as a function of the estimated Si-O-Si bond angles. Dashed lines are fits as guide to the eyes, and the blue dotted line marks the typical damage threshold for pristine HF etched silica.

In our CVD samples, we have observed the vibration from the non-bridging oxygen stretch in the FTIR measurements in the un-treated film compared to the bulk SiO_2. With increasing CO_2 laser treatment temperature, the intensity of this vibration peak can be reduced to a level similar to that of pristine SiO_2. However, the PL spectra from the film (both laser treated and un-treated) did not show any noticeable emission resulted from direct electronic transition of non-bridging oxygen hole centers. The band near 3600 cm^{-1} in the FTIR data (figure 3(b)) also showed that the silanol concentration in the CVD film started high, and decreased significantly after CO_2 laser treatment. Based on these observations, we suggest that the vibration from non-bridging oxygen in as-deposit CVD film is mainly due to Si-OH population. As the film undergoes heat treatment, silanol starts to be driven out through OH diffusion at lower temperatures [28], which explains the decrease in the non-bridging oxygen observed in the FTIR (figure 4(a) and (c)). It is important to point out that this decrease was not monotonic with T_{HT} as the shift in the TO_3 mode is shown figure 4(b). There was a recovery in non-bridging vibration for T_{HT}>1000 K which peaks around ~1600 K (figure 4(a) and (c)), with the effect more moderate for the thinner film (3.1 μm). This increase may be the result of the interaction between molecular water and silica [21]. The fact that we observed an increase in PL at ~450 nm at the wings of CO_2 laser tracks with a peak around T_{HT}=1600 K supports this interpretation. Ultimately, at high enough T_{HT}, the non-bridging mode, as well as PL, decreases again for CO_2 treated CVD films. The structural relaxation and annihilation of the defects is schematically illustrated in figure 10 [29].
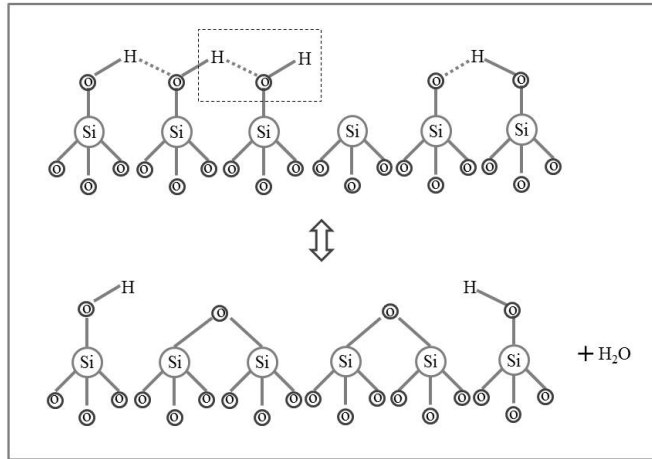
Figure 10: Schematic diagram of the defect annealing mechanisms in CVD films.

This could explain why we are seeing a variation of the non-bridging oxygen population with respect to treatment temperature, but little PL from non-bridging oxygen hole centers. Another feature in the PL spectra worth noting is the peak at ~404 nm, which persists despite of thermal treatment. We believe this is the Raman signal at ~3700 cm^{-1} from the silanol in the wet silica substrate despite of the dehydration of the CVD film resulted from laser treatment.

The onset of the damage threshold change depends strongly on the thickness of the film, with the thickest sample (6.4 μm) only showing a damage threshold increase at ~1900 K, where the underlying substrate also is annealed (figure 7(a)). One possibility for the disparity could be the differences in the thermal profiles through the films. Indeed, the absorption length at 10.6 μm in silica at ~1500 K is about 5.9 μm, implying that heating may not penetrate to the bottom of the 6.4 μm film. However, since thermal diffusion times are long compared to effective dwell times and the beam radius a is large compared to the absorption length, we can treat the laser beam as a CW surface source and estimate the temperature change ΔT as a function of depth z as [30]:

$$\frac{\Delta T(z)}{\Delta T(0)} = erfc\left(\frac{z}{a}\right)\exp\left(\frac{z^2}{a^2}\right)$$

The above expression yields ΔT(6.4 μm)/ ΔT(0)~0.98 or about a 30 K decrease from a surface temperature of 2000 K, far less than the differences observed in the damage threshold data between films. Since the temperature across the film depth was relatively constant for all films, this thickness-related effect on annealing may be attributed to the fact that thicker films contain significantly more defects (for a given density of defects) and therefore require more heating to overcome the population barrier before damage threshold improvement can be observed (i.e. a 'critical mass' effect). For thinner films (1.5 μm and 3.1 μm), on the other hand, the damage threshold first increased gradualy to ~40 J/cm^2 at around T_{HT}=1600 K, similar to the etched silica substrate. The damage threshold improvement is accompanied by a drop in the non-bridging mode intensity. This suggests that in CVD SiO$_2$ film, the population of the ODC type of defects is the main absorber of UV light and may lead to optical damage. However, we note

that while the sampling depth of the TO_3 mode is less than 1 µm due to high absorptivity at ~1120 cm^{-1}, light reflected at ~950 or ~3600 cm^{-1} can probe depths that can include the substrate as well as the film, which may affect the observed intensity changes in these bands. At higher T_{HT} (~1850 K), all film sample damage thresholds improve sharply to ~65 J/cm^2. The fact that this latter increase above the substrate's ~40 J/cm^2 threshold does not vary with film thickness implies a modification of the substrate itself. Moreover, because of the distinctly different T_{HT} dependence of this high damage threshold transition, we postulate that a second mechanism to that of the former damage threshold increase is involved. For example, we note that T_{HT} ~1850 K corresponds to the softening point of fused silica where the viscosity is low enough to allow macroscopic, capillary-driven flow and healing of any residual micro- and nano-crack which limit the fracture toughness of the surface. Further studies are underway to understand this second T_{HT} dependent threshold increase of pristine etched silica surfaces.

In terms of applications, our study also allows one to contemplate the use of CVD for the purposes of damage mitigation by way of additive defect repair for high power laser systems. Indeed, removal or reflow of material for the purpose of damage mitigation has been the focus of virtually every proposed laser-based mitigation attempt thus far, few attempts have been made to replace material lost in the original damage event and thus restore the integrity of the wave propagating media. Indeed, laser-based chemical vapor deposition (L-CVD) is a proven technique for localizing material depositions in standard CVD vacuum chambers which might be used to locally treat isolated damage sites [31]. The study on CVD deposited SiO_2 film on silica substrate may provide a basis for research of using other gas phase silica precursors in L-CVD process, such as tetra ethyl ortho-silicate (TEOS, $Si(OC_2H_5)_4$), to locally deposit high damage threshold silica suitable for high power laser optics.

5. Summary

High purity SiO_2 films deposited using silane-based CVD provides a model system to study the role of the intrinsic defects in laser light absorption and damage. The as-deposited film has high purity and little extrinsic defects such as mechanical fractures, but relatively low laser damage threshold. The FTIR reflectivity measurements show that the film is densified and contains some amount of non-bridging groups most likely in the form of SiOH as opposed to the optically-active non-bridging oxygen hole center, SiO. This is supported by the fact that we observed SiO vibration in FTIR, but little PL due to non-bridging oxygen. Rapid, localized CO_2 laser annealing at temperatures T_{HT}, similar those used in fiber draw processing, relaxes the glass network, enables bond reorganization and reduces PL from glass defects. The damage resistance of the annealed film can be improved as a function of T_{HT} to at least the best processed bulk silica level. The transition of the damage threshold is very sharp and takes place around 1600 K. Below T_{HT}~1600 K, the glass appears to go through mainly the polymerization process. Reorganization of defect bonds kicks in after the glass network is fully relaxed at T_{HT}> 1600 K. Besides the treatment temperature, the translation speed (dwell time) during the laser anneal, and the thickness of the film also affect the post-treatment damage threshold.

LLNL-JRNL-604132

References

[1] Tabak M, Hammer J, Glinsky ME, Kruer WL, Wilks SC, Woodworth J, et al. 1994 Ignition and high-gain with ultrapowerful lasers *Physics of Plasmas* **1** 1626-34

[2] Haynam CA, Wegner PJ, Auerbach JM, Bowers MW, Dixit SN, Erbert GV, et al. 2007 National ignition facility laser performance status *Applied Optics* **46** 3276-303

[3] Bloember.N 1973 Role of cracks, pores, and absorbing inclusions on laser-induced damage threshold at surfaces of transparent dielectrics *Applied Optics* **12** 661-4

[4] Laurence TA, Bude JD, Shen N, Feldman T, Miller PE, Steele WA, et al. 2009 Metallic-like photoluminescence and absorption in fused silica surface flaws *Applied Physics Letters* **94**

[5] Miller PE, Bude JD, Suratwala TI, Shen N, Laurence TA, Steele WA, et al. 2010 Fracture-induced subbandgap absorption as a precursor to optical damage on fused silica surfaces *Optics Letters* **35** 2702-4

[6] Raman RN, Matthews MJ, Adams JJ, Demos SG 2010 Monitoring annealing via CO_2 laser heating of defect populations on fused silica surfaces using photoluminescence microscopy *Opt Express* **18** 15207-15

[7] Skuja L 1994 The origin of the intrinsic 1.9 eV luminescence band in glassy SiO_2 *Journal of Non-Crystalline Solids* **179** 51-69

[8] Matthews MJ, Carr CW, Bechtel HA, Raman RN 2011 Synchrotron radiation infrared microscopic study of non-bridging oxygen modes associated with laser-induced breakdown of fused silica *Applied Physics Letters* **99** 151109

[9] Neauport J, Valla D, Duchesne J, Bouchut P, Lamaignere L, Bigarre J, et al. 2004 Building high damage threshold surfaces at 351 nm *Optical Fabrication, Testing, and Metrology* **5252** 131-9

[10] Mann G, Vogel J, Preuss R, Vaziri P, Zoheidi M, Eberstein M, et al. 2008 Nanosecond laser-induced surface damage of optical multimode fibers and their preforms *Applied Physics a-Materials Science & Processing* **92** 853-7

[11] Brusasco RM, Penetrante BM, Butler JA, Maricle SM, Peterson JE 2002 CO_2 laser polishing for reduction of 351-nm surface damage initiation in fused silica *Laser-Induced Damage in Optical Materials: 2001 Proceedings* **4679** 34-9

[12] Temple PA, Lowdermilk WH, Milam D 1982 Carbon-Dioxide Laser Polishing of Fused-Silica Surfaces for Increased Laser-Damage Resistance at 1064-Nm *Applied Optics* **21** 3249-55

[13] Papernov S, Schmid AW 2002 Correlations between embedded single gold nanoparticles in SiO2 thin film and nanoscale crater formation induced by pulsed-laser radiation *Journal of Applied Physics* **92** 5720

[14] Shackelf.Jf, Studt PL, Fulrath RM 1972 SOLUBILITY OF GASES IN GLASS .2. HE, NE, AND H2 IN FUSED SILICA *Journal of Applied Physics* **43** 1619-&

[15] Suratwala TI, Miller PE, Bude JD, Steele WA, Shen N, Monticelli MV, et al. 2011 HF-Based Etching Processes for Improving Laser Damage Resistance of Fused Silica Optical Surfaces *Journal of the American Ceramic Society* **94** 416-28

[16] Yang ST, Matthews MJ, Elhadj S 2009 Thermal transport in CO_2 laser irradiated fused silica: in situ measurements and analysis *Journal of Applied Physics*

[17] Hue J, Carrec P, Dijon J, Lyan P. R-on-1 automatic mapping: a new tool for laser damage testing In: Soileau MJ, editor. Laser-Induced Damage in Optical Materials Boulder, CO: SPIE; 1995. p. 90-100.

[18] Iacona F, Ceriola G, La Via F 2001 Structural properties of SiO2 films prepared by plasma-enhanced chemical vapor deposition *Materials Science in Semiconductor Processing* **4** 43-6

[19] Tsu DV, Lucovsky G, Davidson BN 1989 Effects of the nearest neighbors and the alloy matrix on SiH stretching vibrations in the amorphous SiOr-H (0<r<2) alloy system *Physical Review B* **40** 1795-805

[20] Almeida RM, Guiton TA, Pantano CG 1990 Characterization of silica-gels by infrared reflection spectroscopy *Journal of Non-Crystalline Solids* **121** 193-7

[21] Theil JA, Tsu DV, Lucovsky G 1990 Reaction patheays and sources of OH groups in low-temperature remote PECVD silicon dioxide thin-films *Journal of Electronic Materials* **19** 209-17

[22] Matthews MJ, Vignes RM, Cooke D, Yang ST, Stolken JS 2010 Analysis of microstructural relaxation phenomena in laser-modified fused silica using confocal Raman microscopy *Optics Letters* **35** 1311-3

[23] Kirk CT 1988 Quantitative-Analysis of the Effect of Disorder-Induced Mode-Coupling on Infrared-Absorption in Silica *Physical Review B* **38** 1255-73

[24] Kucheyev SO, Demos SG 2003 Optical defects produced in fused silica during laser-induced breakdown *Applied Physics Letters* **82** 3230-2

[25] Skuja L 1998 Optically active oxygen-deficiency-related centers in amorphous silicon dioxide *Journal of Non-Crystalline Solids* **239** 16-48

[26] Himpsel FJ, McFeely FR, Talebibrahimi A, Yarmoff JA, Hollinger G 1988 Microscopic Structure Of The SiO_2/Si Interface *Physical Review B* **38** 6084-96

[27] Almeida RM, Pantano CG 1990 Structural Investigation Of Silica-Gel Films By Infrared-Spectroscopy *Journal of Applied Physics* **68** 4225-32

[28] Davis MJ 1999 The effect of water on the viscosity of silicate melts: A configurational entropy approach *Geochimica Et Cosmochimica Acta* **63** 167-73

[29] Brinker CJ, Scherer GW Sol-Gel Science: the Physics and Chemistry of Sol-Gel Processing. Academic Press; 1990.

[30] von Allmen M, Blatter A. Laser-Beam Interactions with Materials. second ed. Hiedelberg: Springer-Verlag; 1998.

[31] Mazumder J, Mohanty PS, Kar A 1996 Mathematical modelling of laser materials processing *International Journal of Materials & Product Technology* **11** 193-252